Guided Waves Along Fluid-Filled Cracks in Elastic Solids and Instability at High Flow Rates

Eric M. Dunham[1]
Assistant Professor
Department of Geophysics and Institute for Computational and Applied Mathematics,
Stanford University,
Stanford, CA 94305
e-mail: edunham@stanford.edu

Darcy E. Ogden
Assistant Professor
Scripps Institution of Oceanography,
University of California, San Diego,
La Jolla, CA 92093
e-mail: dogden@ucsd.edu

We characterize wave propagation along an infinitely long crack or conduit in an elastic solid containing a compressible, viscous fluid. Fluid flow is described by quasi-one-dimensional mass and momentum balance equations with a barotropic equation of state, and the wall shear stress is written as a general function of width-averaged velocity, density, and conduit width. Our analysis focuses on small perturbations about steady flow, through a constant width conduit, at an unperturbed velocity determined by balancing the pressure gradient with drag from the walls. Short wavelength disturbances propagate relative to the fluid as sound waves with negligible changes in conduit width. The elastic walls become more compliant at longer wavelengths since strains induced by opening or closing the conduit are smaller, and the fluid compressibility becomes negligible. As wavelength increases, the sound waves transition to crack waves propagating relative to the fluid at a slower phase velocity that is inversely proportional to the square-root of wavelength. Associated with the waves are density, velocity, pressure, and width perturbations that alter drag. At sufficiently fast flow rates, crack waves propagating in the flow direction are destabilized when drag reduction from opening the conduit exceeds the increase in drag from increased fluid velocity. This instability may explain the occurrence of self-excited oscillations in fluid-filled cracks. [DOI: 10.1115/1.4005961]

1 Introduction

Fluid-filled cracks are ubiquitous in both the natural world and engineering applications. Examples include magma-filled dikes, water-filled crevasses and basal hydraulic fractures beneath glaciers and ice sheets, and induced hydraulic fractures in rock filled with water or hydrocarbons. Seismic waves excited within or around these fractures offer a powerful means of remotely discerning fracture geometry and fluid properties.

Numerous authors have investigated wave propagation in these systems, with special focus on guided waves confined to the vicinity of the fracture surface [1–4]. In this study we confine our attention to planar cracks in an unbounded medium subject to two-dimensional plane strain perturbations (Fig. 1(*a*)). We idealize the crack as an infinitely long, straight conduit of nominally constant width; thus avoiding wave diffraction effects at the crack tips. This geometry supports the existence of dispersive waves known as slow waves or crack waves, for which the dominant restoring force driving wave motion comes not from fluid compressibility but from elasticity of the conduit walls. Additionally, under more restrictive conditions, there are additional modes akin to Rayleigh waves.

Many previous studies have assumed an inviscid fluid initially at rest. In contrast, our reference state involves flow of a viscous fluid at a constant velocity determined by balancing the pressure gradient force with drag from the conduit walls. We find a critical velocity above which crack waves, or in some cases the Rayleigh-like waves, are destabilized. Similar instabilities leading to self-excited oscillations in fluid-filled cracks have been identified previously, first in the context of a lumped-parameter model [5] and later in a more rigorous continuum framework for an incompressible fluid [6], and suggested as an explanation for volcanic tremor. Our present study extends the latter analysis to a compressible fluid.

2 Width-Averaged Model

We restrict attention to wavelengths much larger than the crack width, which permits a width-averaged or quasi-one-dimensional expression of the fluid mass and momentum balance. The governing equations, in conservation form, are

$$\frac{\partial(\rho w)}{\partial t}+\frac{\partial(\rho u w)}{\partial x}=0 \tag{1}$$

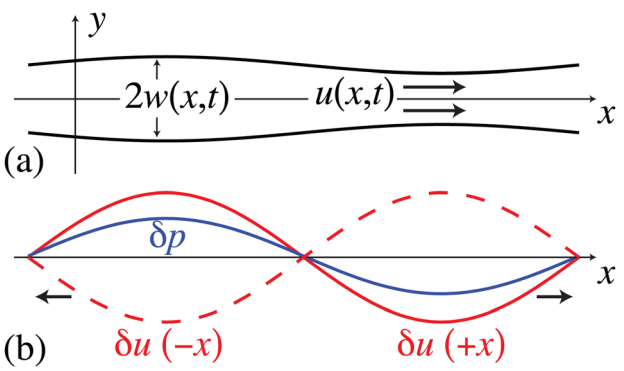

Fig. 1 (*a*) Crack in unbounded elastic solid with opening $2w(x, t)$ containing fluid flowing in $+x$ direction with width-averaged velocity $u(x, t)$. (*b*) Perturbations in pressure (δp) and velocity (δu) carried by sound/crack waves with negligible damping. Waves propagating in the $\pm x$ direction have δu in phase with and of the same sign as $\pm\delta p$. With the linearized equation of state, Eq. (10), density perturbations ($\delta\rho$) have the same sign as δp. For Fourier mode perturbations with phase velocities less than the Rayleigh speed, conduit width perturbations (δw) have the same sign as δp.

[1]Corresponding author.

Contributed by the Applied Mechanics Division of ASME for publication in the Journal of Applied Mechanics. Manuscript received August 21, 2011; final manuscript received January 13, 2012; accepted manuscript posted February 13, 2012; published online April 4, 2012. Assoc. Editor: Nadia Lapusta.

$$\frac{\partial(\rho u w)}{\partial t} + \frac{\partial[(\rho u^2 + p)w]}{\partial x} - p\frac{\partial w}{\partial x} = -\tau \tag{2}$$

for density ρ, conduit half-width w, width-averaged velocity u, pressure p, and wall shear stress τ. Alternatively, Eq. (2) can be written, using Eq. (1), as

$$\rho\left(\frac{\partial u}{\partial t} + u\frac{\partial u}{\partial x}\right) = -\frac{\partial p}{\partial x} - \frac{\tau}{w} \tag{3}$$

If gravity is included, then the pressure gradient term should be replaced by the gradient in hydraulic potential.

We write the wall shear stress in the general form $\tau = \tau(\rho, u, w)$ to encompass the wide range of flow regimes (from laminar to turbulent) that exist at various Reynolds numbers $\rho u w/\mu$, where μ is the fluid viscosity. A widely used expression for turbulent flow is $\tau = f\rho u^2/8$, where f is the Darcy-Weisbach friction factor. An appropriate parametrization at high Reynolds number is [7] the Manning-Strickler relation $f = f_0(\kappa/2w)^{1/3}$, where $f_0 \approx 0.143$ and κ is the wall roughness. Hence,

$$\tau = \frac{f_0}{8}\left(\frac{\kappa}{2w}\right)^{1/3}\rho u^2 \tag{4}$$

In the opposite, low Reynolds number limit of fully developed laminar flow of a linear viscous fluid,

$$\tau = 3\mu u/w \tag{5}$$

The assumption of fully developed flow requires that the time scales of interest (i.e., the wave period in this study) are much larger than the momentum diffusion time across the conduit width ($\sim w^2/(\mu/\rho)$). This limits the applicability of our model and prevents us from properly investigating flow stability in parts of parameter space that might be relevant for explaining volcanic tremor in terms of self-excited oscillations [5,6]. Lifting this restriction requires abandoning the width-averaged flow description, a task that is beyond the scope of the current analysis.

The description of the fluid is completed by an equation of state. We assume a barotropic equation of state, $\rho = \rho(p)$, for which the sound speed is $\sqrt{(d\rho/dp)/\rho}$. This encompasses both isothermal and adiabatic disturbances.

Note that in this model we explicitly account for inertia, compressibility, and drag from the walls (effects that have sometimes been neglected in prior studies). By including them, our model is quite general and we can precisely quantify the conditions under which certain effects can justifiably be ignored to simplify the fluid model. This is particularly the case for fluid compressibility, which can prevent self-excited oscillations by allowing pressure perturbations to be accommodated by compression or expansion of the fluid, rather than by wall deformation.

We are interested in perturbations about steady flow:

$$\rho(x, t) = \rho_0 + \delta\rho(x, t) \tag{6}$$

$$u(x, t) = u_0 + \delta u(x, t) \tag{7}$$

$$p(x, t) = \left(\frac{\partial p}{\partial x}\right)_0 x + \delta p(x, t) \tag{8}$$

$$w(x, t) = w_0 + \delta w(x, t) \tag{9}$$

The unperturbed fields are denoted with subscript 0 and the perturbed fields are preceded by δ. We have assumed for the unperturbed flow that the conduit width is constant; the velocity is sufficiently small, relative to the fluid sound speed, that inertial terms in the momentum balance can be neglected; and changes in density along the conduit are negligible. The dominant balance is thus between the pressure gradient driving the flow and drag, and the steady state velocity u_0 is found by solving $\tau_0 \equiv \tau(\rho_0, u_0, w_0) = -w_0(\partial p/\partial x)_0$.

We next linearize the system of equations by assuming the perturbations are sufficiently small. The linearized equation of state is

$$\delta\rho = \frac{\rho_0}{K_f}\delta p \tag{10}$$

where K_f is the fluid bulk modulus. Using Eq. (10), the linearized mass and momentum balance equations are

$$\frac{D\delta p}{Dt} + \rho_0 c_0^2\frac{\partial \delta u}{\partial x} = -\frac{K_f}{w_0}\frac{D\delta w}{Dt} \tag{11}$$

$$\frac{D\delta u}{Dt} + \frac{1}{\rho_0}\frac{\partial \delta p}{\partial x} = -\frac{\tau_0}{\rho_0 w_0}\left(A_u\frac{\delta u}{u_0} + A_\rho\frac{\delta p}{K_f} - A_w\frac{\delta w}{w_0}\right) \tag{12}$$

in which $c_0 \equiv \sqrt{K_f/\rho_0}$ is the sound speed and $D/Dt \equiv \partial/\partial t + u_0\partial/\partial x$ is the rate of change of a quantity in a frame of reference comoving with the unperturbed flow. The right side of Eq. (11) captures the influence of conduit width fluctuations on the mass balance.

Similarly, the right side of Eq. (12) reflects changes in drag due to perturbations in ρ, u, and w, in terms of the dimensionless factors A_u, A_w, and A_ρ defined in Table 1. The velocity dependence of drag introduces the characteristic damping rate

$$\alpha \equiv \frac{A_u\tau_0}{2\rho_0 u_0 w_0} \tag{13}$$

such that α^{-1} is the time scale over which waves are expected to decay in the absence of drag perturbations from density and conduit width perturbations. For example, $\alpha^{-1} \sim w_0^2/(\mu/\rho_0)$ for the viscous drag law, which is simply the momentum diffusion time across the conduit width. Relevant properties of the drag laws are summarized in Table 1.

The system of equations is closed by the elastic response coupling δw to perturbations in the other fields. For quasi-static elasticity,

$$\delta p(x, t) = \frac{G^*}{\pi}\int_{-\infty}^{\infty}\frac{\partial \delta w(x', t)/\partial x'}{x - x'}dx' \tag{14}$$

where $G^* \equiv G/(1-\nu)$ for shear modulus G and Poisson's ratio ν. The corresponding result for elastodynamics is presented in the following section. All examples in this study are for a Poisson solid ($\nu = 1/4$).

3 Origin of Wave Motion

Wave motion in this system arises from two effects. Waves carry pressure perturbations, and the system accommodates these

Table 1 Properties of drag laws

Parameter	Viscous, Eq. (5)	Turbulent, Eq. (4)
$A_u \equiv \frac{u\partial\tau}{\tau\partial u}$	1	2
$A_w \equiv 1 - \frac{w\partial\tau}{\tau\partial w}$	2	4/3
$A_\rho \equiv \frac{\rho\partial\tau}{\tau\partial\rho}$	0	1
$m \equiv 2A_w/A_u$	4	4/3
$n \equiv 2A_\rho/A_u$	0	1
α	$\frac{3\mu}{2\rho_0 w_0^2}$	$\frac{f_0}{8}\left(\frac{\kappa}{2w_0}\right)^{1/3}\frac{u_0}{w_0}$

pressure changes either by compressing and expanding the fluid, or by opening and closing the conduit walls. The first effect is quantified by the fluid compressibility,

$$\beta_f \equiv \frac{1}{\rho}\left(\frac{\partial \rho}{\partial p}\right)_w = \frac{1}{K_f} \tag{15}$$

where the subscript w on the partial derivative indicates that conduit width is held fixed. The associated wave speed is the sound speed $c_0 \equiv 1/\sqrt{\rho_0 \beta_f}$.

The second source of wave motion comes from the restoring force offered by elastic deformation of the conduit walls. Elasticity links conduit width perturbations to pressure perturbations. We consider the full elastodynamic response, with the quasi-static response emerging as a limit.

Describing the elastic response, as well as assessing stability and examining wave motions, is facilitated by seeking modal solutions of the form

$$\delta p(x, t) = \delta \hat{p}(k, s)\exp(ikx + st) \tag{16}$$

with similar notation applying to other fields. The perturbation wavelength is $\lambda \equiv 2\pi/|k|$. The phase velocity of the perturbation is $c \equiv -\mathrm{Im}(s)/k$ and the growth/decay rate is $\mathrm{Re}(s)$. The quasi-static response, Eq. (14), transforms to $\delta \hat{p}(k, s) = G^*|k|\delta \hat{w}(k, s)$. The elastodynamic response introduces the P- and S-wave speeds of the solid, c_p and c_s, respectively, and generalizes this expression to [8]

$$\delta \hat{p}(k, s) = \frac{G^*|k|}{F(k, s)}\delta \hat{w}(k, s), \quad F(k, s) \equiv \frac{\alpha_p(1-\alpha_s^2)}{(1-\nu)R} \tag{17}$$

in which $\alpha_s \equiv \sqrt{1+(s/kc_s)^2}$, $\alpha_p \equiv \sqrt{1+(s/kc_p)^2}$, and $R \equiv 4\alpha_s\alpha_p - (1+\alpha_s^2)^2$ is the Rayleigh function. The appropriate Riemann sheet for the square roots is that for which $\mathrm{Re}\ \alpha_p \geq 0$ and $\mathrm{Re}\ \alpha_s \geq 0$, which keeps fields from diverging with increasing distance from the conduit. For α_s, branch cuts in the complex s plane extend between ikc_s and $i\infty$, and $-ikc_s$ and $-i\infty$, and likewise for α_p. (For more details, see Ref. [8].) Furthermore, we have defined the function F such that $F \to 1$ as $|s/kc_s| \to 0$ (i.e., in the quasi-static limit). Figure 2 illustrates properties of $F(k, s)$ along the imaginary axis for phase velocities between zero and the S-wave speed.

More precise versions of Eqs. (14) and (17) would also include coupling between wall shear stress and conduit opening. While easily included, dimensional analysis reveals that this effect is several orders of magnitude smaller than the pressure-width coupling and we thus neglect it.

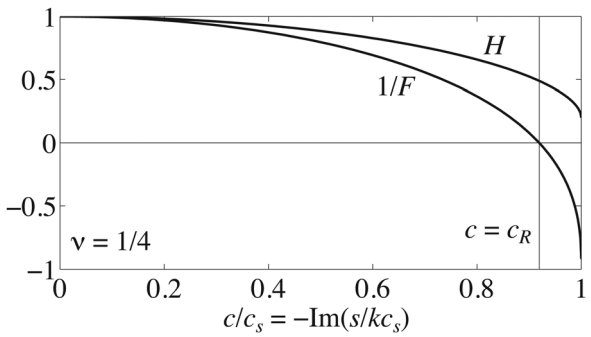

Fig. 2 Plot of $1/F$ (Eq. (17)) and H (Eq. (25)) as a function of phase velocity $c = -\mathrm{Im}(s)/k$ for purely imaginary s, shown for $\nu = 1/4$. For propagating waves, the ratio of conduit compressibility to fluid compressibility is $F(k, s)\Lambda$, where Λ is the quasi-static compressibility ratio defined in Eq. (20). Note that F is singular at the Rayleigh speed ($c = c_R$), making the conduit extremely compliant for waves propagating near this speed.

Equation (17) serves to define the conduit compressibility in the quasi-static limit as:

$$\beta_w \equiv \frac{1}{w}\left(\frac{\partial w}{\partial p}\right)_\rho = \frac{1}{G^*|k|w_0} \tag{18}$$

The conduit is more compliant for longer wavelength deformations since the restoring stresses are proportional to the strains $\sim \delta\hat{w}/\lambda$. The dynamic compressibility is $F(k, s)\beta_w$. As seen in Fig. 2, this can be quite large for waves propagating near the Rayleigh speed, c_R, since near that speed, opening and closing of the walls occurs with negligible pressure perturbations.

Associated with the quasi-static conduit compressibility, Eq. (18), is the wave speed

$$c_w \equiv \frac{1}{\sqrt{\rho_0 \beta_w}} = \sqrt{\frac{G^*|k|w_0}{\rho_0}} \tag{19}$$

which decreases with increasing wavelength. This expression is analogous to the Moens–Korteweg speed governing wave propagation in a thin-walled elastic tube filled with an incompressible, inviscid fluid [9].

The relative importance of the two mechanisms that generate wave motions is captured by the dimensionless compressibility ratio. This is

$$\Lambda \equiv \frac{\beta_w}{\beta_f} = \frac{K_f}{G^*|k|w_0} \tag{20}$$

in the quasi-static case, and $F(k, s)\Lambda$ in the more general dynamic case. Equation (20) also serves to define the quasi-static "elastic coupling length," $\lambda_{el} \equiv 2\pi w_0 G^*/K_f$, such that $\Lambda = \lambda/\lambda_{el}$ is a dimensionless measure of the perturbation wavelength.

At short wavelengths ($\Lambda \ll 1$) the conduit walls are effectively rigid and we expect to find nondispersive sound waves propagating at speed c_0. In the opposite limit ($\Lambda \gg 1$), pressure fluctuations are accommodated almost entirely by opening or closing of the conduit and the fluid is effectively incompressible, and for quasi-static elasticity, waves are expected to propagate at speed c_w as given in Eq. (19).

We will shortly demonstrate the existence of waves with phase velocities varying continuously between c_0 and c_w as a function of Λ. Such waves have previously been identified in studies of fluid-filled cracks [2,3], where they were termed slow waves (since $c_w \ll c_0$ for $\Lambda \gg 1$) or crack waves. We adopt the latter terminology in this work.

4 Characteristic Equation

For modal perturbations of the form of Eq. (16), we can write Eqs. (11), (12), and (17) as the dimensionless homogeneous system

$$(S + iM_0)\frac{\delta \hat{p}}{K_f} + i\frac{\delta \hat{u}}{c_0} = -(S + iM_0)\frac{\delta \hat{w}}{w_0} \tag{21}$$

$$(S + iM_0)\frac{\delta \hat{u}}{c_0} + i\frac{\delta \hat{p}}{K_f} = -2\zeta\frac{\delta \hat{u}}{c_0} - M_0\zeta\left(n\frac{\delta \hat{p}}{K_f} - m\frac{\delta \hat{w}}{w_0}\right) \tag{22}$$

$$\frac{\delta \hat{w}}{w_0} = \Lambda F(S)\frac{\delta \hat{p}}{K_f} \tag{23}$$

in which $S \equiv s/kc_0$, $M_0 \equiv u_0/c_0$ is the Mach number of the unperturbed flow, $\zeta \equiv \alpha/kc_0$ is the dimensionless damping ratio, $m \equiv 2A_w/A_u$ and $n \equiv 2A_\rho/A_u$. Table 1 lists m and n for several drag laws. Furthermore, we have recognized that $F(k, s)$ depends

on k and s only through their ratio, permitting us to write F with only a single argument, $F=F(S)$, in the above expression and all subsequent ones.

In this notation, undamped sound waves propagating at speed c_0 relative to the steady flow satisfy $S+iM_0=\mp i$. In this expression for S and all subsequent ones, the top sign will be associated with waves propagating with the flow and the bottom sign with waves propagating against it. Of course, for sufficiently large M_0 it is possible that both waves propagate in the $+x$ direction. Some caution must be employed when taking the incompressible fluid limit: while both c_0 and Λ approach infinity, the ratio $c_0/\sqrt{\Lambda}\equiv c_w$ remains constant and provides the relevant velocity scale.

A nontrivial solution of Eqs. (21)–(23) exists only when the determinant of the coefficient matrix vanishes. The resulting characteristic equation is

$$(S+iM_0)^2+2\zeta(S+iM_0)+\frac{1}{1+\Lambda F(S)}+iM_0\zeta\frac{m\Lambda F(S)-n}{1+\Lambda F(S)}=0 \tag{24}$$

When $M_0=0$ and $\zeta=0$, Eq. (24) matches the dispersion equation for crack waves in an inviscid, motionless fluid derived by Paillet and White [1] (their Eq. (3) in the $|k|w_0\ll 1$ limit) and independently by Ferrazzini and Aki [3] (their Eq. (14*b*) in the $|k|w_0\ll 1$ limit).

As the Rayleigh function has only two roots on the proper Riemann sheet, the function $F(S)$ can be factored by introducing [10]

$$H(S)\equiv F(S)\left[1+(S/S_R)^2\right] \tag{25}$$

where $\mp iS_R$ are the Rayleigh poles ($S_R\equiv c_R/c_0$ where c_R is the Rayleigh-wave speed). The function $H(S)$ is analytic in the complex S plane except across branch cuts along the imaginary axis, and $H(S)\approx 1$ when $|S|\ll S_R$ (i.e., in the quasi-static limit); see Fig. 2. Equation (24) can thus be written as

$$D(S)\equiv\left[1+(S/S_R)^2+\Lambda H(S)\right]\left[(S+iM_0)^2+2\zeta(S+iM_0)\right]+(1-inM_0\zeta)\left[1+(S/S_R)^2\right]+imM_0\zeta\Lambda H(S)=0. \tag{26}$$

This characteristic equation or dispersion relation constitutes the main result of our analysis and the remainder of this manuscript is devoted to studying its solutions.

5 Solutions of the Characteristic Equation

We now discuss the various wave solutions of Eq. (26). The limiting case of no fluid-solid coupling (Sec. 5.1) provides a foundation that facilitates understanding of the more complex solutions that emerge from interactions between the elastic and acoustic systems. Section 5.2 focuses on crack waves and the conditions under which unstable growth of these wave modes leads to self-excited oscillations. This section contains the most important results of this study. We complete our investigation by discussing other solutions in Sec. 5.3, though these are generally less interesting and relevant than the crack waves studied in the previous section.

5.1 No Fluid-Solid Coupling. First consider the limiting case $\Lambda\to 0$ (the short wavelength limit), for which there are no interactions between the fluid and solid. Equation (26) can be factored as

$$\left[1+(S/S_R)^2\right]\left[(S+iM_0)^2+2\zeta(S+iM_0)+1-inM_0\zeta\right]=0 \tag{27}$$

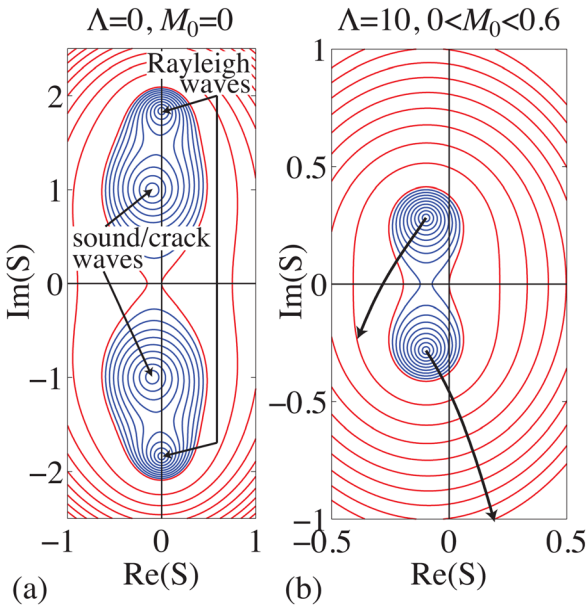

Fig. 3 Contours of $|D(S)|$ in complex S plane, with $D(S)$ defined in Eq. (26). Blue lines are contours from 0.1 to 1, plotted every 0.1; red lines continue from 1 up, with spacing of 1. Shown for $c_s/c_0=2$, $\zeta=0.1$, and $\nu=1/4$. (*a*) For $\Lambda=0$ and $M_0=0$, solutions of $D(S)=0$ are Rayleigh waves and damped sound waves. (*b*) Contours plotted for $\Lambda=10$ and $M_0=0$. Black curves show trajectories of crack wave solutions as M_0 is increased from 0 to 0.6 for viscous drag law (Table 1, $m=4$, $n=0$). The wave propagating with the flow becomes unstable beyond a critical M_0.

and there are four solutions (Fig. 3(*a*)). Two are neutrally stable Rayleigh waves, $S=\mp iS_R$, and two are damped sound waves propagating relative to the moving fluid,

$$S+iM_0=\mp i\sqrt{1-\zeta^2-inM_0\zeta}-\zeta \tag{28}$$

The latter solutions owe their existence to fluid compressibility, and are damped since drag increases with fluid velocity. Figure 1(*b*) illustrates properties of the sound wave solutions with small damping ($\zeta\ll 1$), in particular the relative signs and phases of the various fields.

When $n=0$ (i.e., when drag is independent of density, as for the viscous drag law), Eq. (28) is the standard frequency equation for a damped harmonic oscillator with damping ratio ζ. ζ measures the amplitude decay over the wave period, which can alternatively be expressed in terms of the quality factor $Q\equiv(2\zeta)^{-1}$. For $\zeta\ll 1$, the waves propagate relative to the moving fluid at approximately the fluid sound speed c_0 and are damped at approximately the rate α. When the system is overdamped ($\zeta>1$), perturbations cease to propagate relative to the fluid and simply decay in time.

When $n>0$, the damping rate and phase velocity are altered. Assuming this is a small effect ($nM_0\zeta\ll 1-\zeta^2$) and that we are in the underdamped limit ($\zeta<1$), only the damping rate is modified to first order, from $-\alpha$ when $n=0$ to $-\alpha(1\pm nM_0/2\sqrt{1-\zeta^2})$. Hence the wave propagating with the flow (the top sign) decays slightly faster, while the wave opposing flow (the bottom sign) decays slightly less rapidly. Figure 1(*b*) helps explain the origin of this effect. The wave propagating with the flow carries velocity and density perturbations of the same sign, both of which increase drag. Drag perturbations from velocity and density perturbations instead oppose each other for the wave propagating in the opposite direction, leading to diminished damping.

5.2 Crack Waves and Instability Condition. Now we include fluid-solid coupling and focus on the crack wave solutions for nonzero Λ, which are generalizations of the sound wave solutions that exist in the $\Lambda \to 0$ limit. We examine properties of these crack waves and show that they become unstable for sufficiently fast fluid velocity u_0.

We first assume that the relevant solutions have phase velocities much less than the elastic wave speeds. This is always the case if $c_s/c_0 \gg 1$. Because crack waves are expected to have phase velocities of order $c_w \equiv c_0/\sqrt{\Lambda}$, the assumption is also valid for arbitrary c_s/c_0 (even $c_s/c_0 < 1$) if Λ is sufficiently large. Therefore the elastic response is effectively quasi-static for these waves, permitting us to approximate $1+(S/S_R)^2 \approx 1$ and $H(S) \approx 1$ (see Fig. 2) in the characteristic equation, Eq. (26). The solutions thus satisfy

$$(S+iM_0)^2 + 2\zeta(S+iM_0) + \frac{1}{1+\Lambda} + iM_0\zeta\frac{m\Lambda - n}{1+\Lambda} = 0 \qquad (29)$$

The last term on the left side of Eq. (29) captures the drag perturbations from conduit width and density changes; the former leads to instability under conditions identified below.

Before discussing that instability, consider the simpler case where that term can be neglected (e.g., for sufficiently small M_0). We find

$$S + iM_0 \approx \mp i\sqrt{1/(1+\Lambda) - \zeta^2} - \zeta \qquad (30)$$

Comparison with the rigid-wall sound wave solution, Eq. (28), suggests that these crack waves are generalizations of damped sound waves, with reduced phase velocity due to the additional system compliance arising from wall deformation. The relative signs and phases of the fields, for $\zeta \ll 1$, are identical to those of sound waves (Fig. 1(*b*)).

Since the walls are more deformable at longer wavelengths, crack waves exhibit anomalous dispersion, with shorter wavelength waves ($\Lambda \ll 1$) propagating at the damped fluid sound speed. The longer wavelength waves ($\Lambda \gg 1$) satisfy $S + iM_0 \approx \mp i\sqrt{1/\Lambda - \zeta^2} - \zeta$. Without damping, $S + iM_0 \approx \mp i/\sqrt{\Lambda}$. Restoring dimensions, the phase velocity relative to the fluid becomes the crack wave speed $c_w \equiv c_0/\sqrt{\Lambda}$ for an inviscid, incompressible fluid defined in Eq. (19). All dependence on fluid compressibility and the fluid sound speed vanishes, indicating that in this limit the restoring force responsible for wave motion comes solely from wall deformation and the fluid is effectively incompressible. As with sound waves, when damping is present and exceeds a critical value ($\zeta > 1/\sqrt{1+\Lambda}$), the waves become overdamped and cease to propagate.

When M_0 is not sufficiently small that the last term on the left side of Eq. (29) can be neglected, the solutions are

$$S + iM_0 = \mp i\sqrt{\frac{1}{1+\Lambda} - \zeta^2 + iM_0\zeta\frac{m\Lambda - n}{1+\Lambda}} - \zeta \qquad (31)$$

The wave propagating against the flow (the bottom sign) is always stable. In contrast, the wave propagating with the flow (the top sign) becomes unstable if

$$M_0 \equiv \frac{u_0}{c_0} > \frac{2\sqrt{1+\Lambda}}{m\Lambda - n} \quad \text{or} \quad \frac{u_0}{c_w} > \frac{2\sqrt{1+1/\Lambda}}{m - n/\Lambda} \qquad (32)$$

which is shown in Fig. 4. For $\Lambda \gg 1$, this instability condition becomes $u_0 > (2/m)c_w$, which is independent of c_0 (as expected in this incompressible fluid limit). Remarkably, the instability condition is independent of the damping ratio ζ, although the growth rate does depend on ζ.

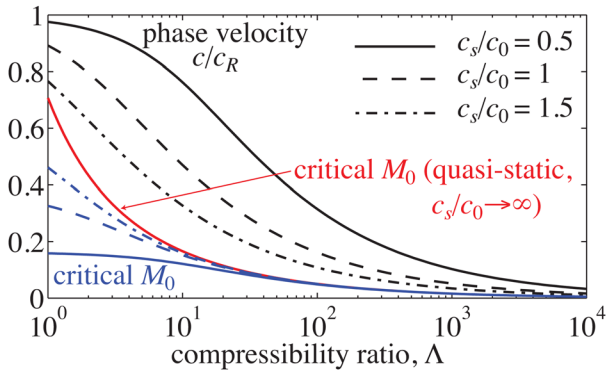

Fig. 4 Critical Mach number, $M_0 \equiv u_0/c_0$, for instability, shown for viscous drag law (Table 1, $m=4$, $n=0$). Red curve is for quasi-static elasticity (Eq. (32)) and blue curves show corresponding values with full elastodynamic response for several values of c_s/c_0. Black curves show phase velocity c at neutral stability, which approaches but never exceeds the Rayleigh speed c_R.

Figure 1(*b*) helps explain the origin of the instability. The wave propagating with the flow carries velocity and pressure perturbations of the same sign. For quasi-static elasticity, the conduit width perturbations are of the same sign as the pressure perturbations. Hence, where velocity is largest, the conduit is widest. Instability occurs if the drag reduction from opening the conduit exceeds the additional drag from the faster flow.

When $c_s/c_0 \gg 1$, the quasi-static elasticity approximation is well justified for crack waves of all wavelengths. This is no longer the case if the crack wave phase velocity becomes comparable to elastic wave speeds, as occurs for smaller values of c_s/c_0. To investigate this case, solutions are obtained by numerically solving the characteristic equation, Eq. (26). For large values of Λ, the crack waves have sufficiently reduced phase velocities that the elastic response is effectively quasi-static, even if $c_s/c_0 < 1$. Hence the critical M_0 for instability is identical to that found in the quasi-static analysis (Fig. 4). As Λ decreases, we expect the system to become stiffer and the crack wave phase velocity to increase. Opposing this is an increase in elastic compliance for phase velocities approaching the Rayleigh speed (Fig. 2). The net effect is that the crack wave phase velocity asymptotically approaches, but never surpasses, the Rayleigh wave speed of the solid as Λ decreases, even if $c_w > c_R$. Furthermore, the critical M_0 for instability is reduced relative to its quasi-static value (Fig. 4). This is because at phase velocities near the Rayleigh speed, only small pressure changes are required for substantial wall deformation, with the latter process promoting instability through drag reduction. The critical M_0 again appears to be independent of ζ.

5.3 Additional Solutions. We continue by discussing Rayleigh solutions for arbitrary Λ (i.e., the generalizations of the Rayleigh waves found in the $\Lambda \to 0$ limit). We first assume that $c_s/c_0 > 1$ (since the phenomenology changes rather dramatically when $c_s/c_0 < 1$). Our general result is that Rayleigh solutions exist only for small values of Λ and are never unstable. We then proceed to the more complicated $c_s/c_0 < 1$ case, where the distinction between crack wave and Rayleigh solutions is less clear.

We initially assume $c_s/c_0 > 1$, $M_0 = 0$, and $\zeta = 0$. As can be verified *a posteriori*, the Rayleigh solutions for nonzero Λ, if they exist, have purely imaginary S with phase velocity $c = ic_0 S$ satisfying $c_R < |c| < c_s$ (i.e., they are neutrally stable waves with phase velocities between the Rayleigh and S-wave speeds). A useful way to write the characteristic equation, Eq. (26), is thus

$$(c/c_R)^2 = 1 + \frac{\Lambda H(-ic/c_0)}{1-(c_0/c)^2} \qquad (33)$$

which shows clearly that $c = \pm c_R$ when $\Lambda = 0$ (a result that remains true even if $\zeta \neq 0$). Since $H(S)$ is positive for $c_R < |c| < c_s$ (Fig. 2) and $c_0/|c| < 1$, the last term on the right side of Eq. (33) is positive real. Thus c must increase from c_R at $\Lambda = 0$ to c_s at $\Lambda = \sqrt{2}(1-\nu)^{3/2}[1-(c_0/c_s)^2]$ (an expression attained by evaluating the characteristic equation at $c = c_s$). When $c_0/c_s \ll 1$ and $\nu = 1/4$, the maximum $\Lambda \approx 0.92$ (a limit which decreases for larger c_0/c_s). We verify, via numerical calculations, that the Rayleigh solutions cease to exist for larger Λ. A similar phenomenology also holds for $\zeta > 0$ and $M_0 > 0$, except that the Rayleigh solutions are damped (though only mildly—in all cases studied, $-1 \ll \mathrm{Re}(S) \leq 0$, regardless of the value of ζ).

When $c_s/c_0 < 1$ we again generally find four solutions, two with phase velocities close to the Rayleigh speed and two similar to sound waves. In this section, we provide some discussion of these solutions, particularly in certain limits, but caution that the interplay between elastodynamics and acoustics is quite complicated and a more thorough investigation is likely warranted.

We first consider the $c_s/c_0 \ll 1$ limit. We expect sound waves to have $|S| \sim 1 \gg S_R$. Since $F(S) \to 0$ as $|S|/S_R \to \infty$, then the characteristic equation, Eq. (24), has solutions identical to the rigid-wall sound wave solutions, Eq. (28). That is simply because the elastic waves are so slow in this limit that the walls cannot deform over the time scales associated with sound waves. Numerical results indicate that these solutions only exist for small Λ.

Rayleigh solutions in the $c_s/c_0 \ll 1$ limit are expected to have $|S| \sim S_R \ll 1$. For $M_0 = 0$ and $\zeta > 0$, the characteristic equation simplifies to

$$1 + (S/S_R)^2 + 2\zeta S \Lambda H(S) \approx 0 \tag{34}$$

The solutions have phase velocities close to c_R and are slightly damped. When $M_0 > 0$, the wave propagating against the flow becomes damped at a faster rate, while the wave propagating in the flow direction can become unstable.

We also point out properties of the Rayleigh solutions in the more general case of $c_s/c_0 < 1$ but not necessarily $c_s/c_0 \ll 1$. When $M_0 = 0$ and $\zeta = 0$, the waves are neutrally stable. The analysis leading up to Eq. (33) applies also to this case, except that the last term on the right side of Eq. (33) is negative real. Consequently, solutions exist for all Λ, and their phase velocity decreases from c_R at $\Lambda = 0$ toward zero as Λ increases.

We note one final aspect of the solutions with regard to their evolution as the wave speed ratio passes the transitional region $c_s/c_0 \sim 1$. We have encountered several qualitatively different behaviors, two of which are illustrated in Fig. 5.

If Λ is sufficiently small (as is the case in Fig. 5), then both crack waves and Rayleigh waves exist for $c_s/c_0 > 1$. The Rayleigh waves have phase velocity $c = c_R$ when $c_s/c_0 \gg 1$. As c_s/c_0 decreases, the normalized phase velocity of the Rayleigh solution, c/c_s, increases. For small values of ζ (Fig. 5(*a*)), the phase velocity approaches an asymptotic value close to c_0/c_s (specifically the damped sound speed defined in Eq. (28), as discussed previously). Thus what was classified as the Rayleigh solution for $c_s/c_0 > 1$ becomes the sound wave solution for $c_s/c_0 < 1$. In addition, the crack wave solution for $c_s/c_0 > 1$ has a normalized phase velocity, c/c_0, that decreases with decreasing c_s/c_0. When $c_s/c_0 < 1$, the phase velocity of this solution asymptotically approaches c_R/c_0, thus becoming the solution we have classified as the Rayleigh solution in this section. We therefore see the terminology only applies away from $c_s/c_0 \sim 1$, and that when ζ is small the two types of solutions switch as c_0/c_s passes through this transitional region.

For larger values of ζ (Fig. 5(*b*)), the Rayleigh solution for $c_s/c_0 > 1$ remains the Rayleigh solution for $c_s/c_0 < 1$, and the crack wave for $c_s/c_0 > 1$ transitions to the sound wave solution for $c_s/c_0 < 1$. In both cases, the Rayleigh solution propagating with the flow becomes unstable, at high M_0, for a range of c_s/c_0 approximately centered around M_0. The instability is more pronounced (i.e., $\mathrm{Re}(S)$ is larger) if ζ is larger.

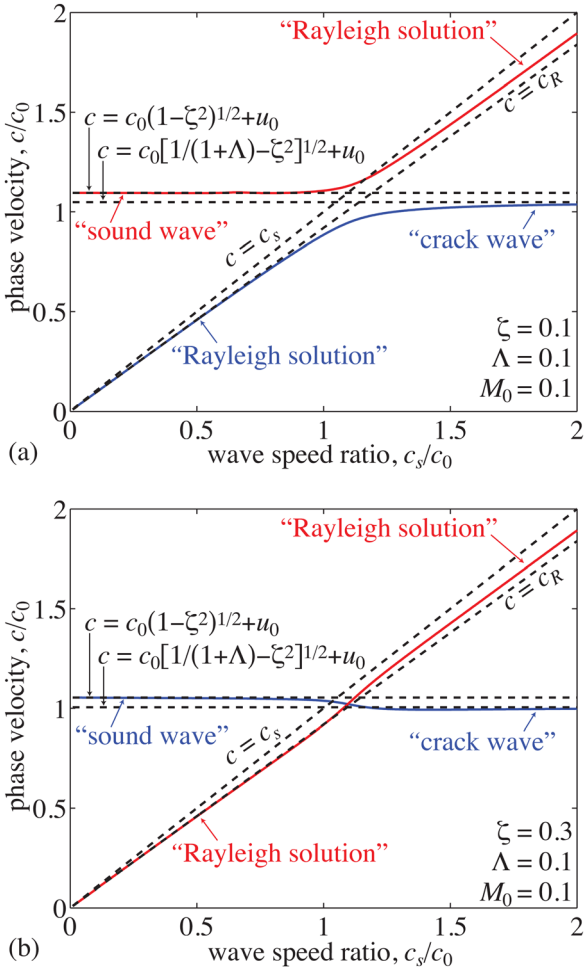

Fig. 5 Phase velocity of solutions propagating with flow (red and blue curves, with terminology in quotes), as a function of c_s/c_0. Dashed black lines labeled $c = \ldots$ show limiting speeds. Shown for viscous drag law (Table 1) with $M_0 = 0.1$ and $\Lambda = 0.1$. Solution trajectories through transition region $c_s/c_0 \sim 1$ differ for (*a*) $\zeta = 0.1$ and (*b*) $\zeta = 0.3$.

The above phenomenology applies when Λ is small (generally $\Lambda \lesssim 1$, though this is not a particularly precise bound). At larger values of Λ, the Rayleigh solution for $c_s/c_0 > 1$ only exists for c_s/c_0 above a threshold value, if it exists at all. When it does exist, then as c_s/c_0 decreases, the normalized phase velocity c/c_s of this solution increases from c_R/c_s to just above unity, as described around Eq. (33), at which point the solution ceases to exist.

At these larger values of Λ, the crack wave solution for $c_s/c_0 > 1$ continuously transitions to the Rayleigh solution for $c_s/c_0 < 1$, similar to the case shown in Fig. 5(*a*), for small ζ. For larger ζ, the crack wave transitions to the sound wave solution, as in Fig. 5(*b*). In addition, for these larger values of ζ, the Rayleigh solution often exists, but only for c_s/c_0 below a critical value around unity.

6 Discussion

We have characterized guided waves in fluid-filled cracks, and identified an instability associated with certain wave modes that appears when the fluid velocity exceeds a threshold. The system is most prone to instability when pressure changes are primarily accommodated by wall deformation and not fluid compressibility (i.e., in the large Λ limit). The analysis framework permits broad application to flow regimes ranging from laminar flow of a viscous fluid to turbulent flows. However, for viscous fluids (Table 1), the assumption of fully developed flow restricts

application of our model to long period or highly damped waves. In terms of the dimensionless variables, this condition is $\zeta \gtrsim 1/\sqrt{1+\Lambda}$.

Unfortunately, this prevents us from rigorously assessing the viability of this model in explaining volcanic tremor as self-excited oscillations from magma flowing through dikes, as the most relevant parts of parameter space do not quite satisfy this restriction. Dikes with $w \sim 1$ m filled with basalt ($\mu/\rho \sim 10^{-2} - 1$ m^2/s) have damping rate $\alpha \sim 10^{-2} - 1$ s^{-1}. Typical rock and magma properties result in an elastic coupling length $\lambda_{el} \sim 10$ m, at least at depths where gas exsolution is minimal and magma is primarily liquid melt. Wavelengths of interest approach $\sim$1 km, giving $\Lambda \sim 100$ and $\zeta \sim 10^{-3} - 10^{-1}$. For these parameters, the relevant restoring force for waves comes from wall deformation rather than fluid compressibility, such that crack waves propagate at speed $c_w \sim 100$ m/s. The elastic response is effectively quasi-static so the instability condition is $u_0 > 0.5 c_w \sim 50$ m/s. These velocities are an order of magnitude larger than typically inferred in fissure eruptions, especially at depth. Closer to the surface, gas exsolution leads to larger velocities, but decreased Λ due to increased fluid compressibility.

Narrower dikes have larger conduit compressibility β_w and thus Λ, making the system more prone to instability. However, the steady flow velocity u_0 would be substantially reduced for a given pressure gradient due to increased drag. If instead of magma, we consider steam or other hydrothermal fluids [6], the fluid compressibility will be larger, thereby decreasing Λ and increasing the threshold velocity for instability well above expected values.

Harmonic tremor has presumably also been observed on ice sheets during rapid subglacial lake drainage events [11]. We tentatively apply our model to hydraulic fractures along the ice-rock interface, although this violates our assumption that the crack separates identical elastic half-spaces. Proceeding nonetheless, for interesting parts of parameter space, Λ is sufficiently large that crack wave speeds are well below the elastic wave speed and the elastic response is quasi-static. For the turbulent flow law (Table 1) in this limit, the instability condition is $u_0 > 1.5 c_w$. Taking $\rho_0 \approx 1000$ kg/m^3 and $G^* \approx 5$ GPa,

$$c_w \sim 180 \left(\frac{100 \text{ m}}{\lambda}\right)^{1/2} \left(\frac{w_0}{0.1 \text{ m}}\right)^{1/2} \text{m/s} \tag{35}$$

The predicted u_0 for instability is one or two orders of magnitude larger than inferred subglacial fluid velocities [7]. Furthermore, $\zeta \ll 1$ so predicted growth rates of the instability would be quite low, even if it were to exist.

We therefore tentatively conclude that seismic tremor observed in both volcanoes and glaciers is unlikely to arise from self-excited oscillations via the crack wave instability we have identified. However, we do speculate that crack waves likely play a central role in tremor, as has been suspected in volcanic systems for many years [2,3]. In the absence of self-excitation, sustained perturbations from disturbances in either the fluid or solid (bursting of gas bubbles or fracture of conduit walls, for example) are required to continually excite crack waves. Investigations into potential excitation mechanisms and their observational signatures are warranted.

Acknowledgment

We thank Leif N. Thomas for valuable discussions in the early stages of this work. This work was supported by NSF Grant No. EAR-1114073.

Nomenclature

$D(S)$ = characteristic equation
$F(S)$ = elastodynamic transfer function
G = solid shear modulus
$H(S)$ = elastodynamic transfer function after removal of Rayleigh poles
K_f = fluid bulk modulus
$M_0 \equiv u_0/c_0$ = Mach number
$S \equiv s/kc_0$ = nondimensional perturbation time dependence
$S_R \equiv c_R/c_0$ = wave-speed ratio
$c \equiv \text{Im}(s)/k$ = phase velocity of perturbation
$c_0 \equiv \sqrt{K_f/\rho_0}$ = fluid sound speed
c_p = solid P-wave speed
c_R = solid Rayleigh-wave speed
c_s = solid S-wave speed
c_w = crack wave phase velocity for incompressible, inviscid fluid
k = perturbation wavenumber
m = dependence of τ on w
n = dependence of τ on ρ
$p(x,t)$ = fluid pressure
s = perturbation time dependence
t = time
x = distance along crack
$u(x, t)$ = fluid velocity (width-averaged)
$w(x, t)$ = conduit half-width
α = damping rate
β_f = fluid compressibility
β_w = conduit compressibility
$\delta(\cdot)$ = perturbed field $(\cdot)$
λ = perturbation wavelength
Λ = quasi-static compressibility ratio
μ= fluid viscosity
ν = solid Poisson's ratio
$\rho(x, t)$ = fluid density
$\tau(x, t)$ = wall shear stress
ζ = damping ratio
$(\cdot)_0$ = unperturbed field $(\cdot)$

References

[1] Paillet, F. L., and White, J. E., 1982, "Acoustic Modes of Propagation in the Borehole and Their Relationship to Rock Properties," Geophys., **47**(8), pp. 1215–1228.
[2] Chouet, B., 1986, "Dynamics of a Fluid-Driven Crack in Three Dimensions by the Finite Difference Method," J. Geophys. Res., **91**(B14), pp 13,967–13, 992.
[3] Ferrazzini, V., and Aki, K., 1987, "Slow Waves Trapped in a Fluid-Filled Infinite Crack: Implications for Volcanic Tremor," J. Geophys. Res., **92**(B9), pp. 9215–9223.
[4] Korneev, V., 2008, "Slow Waves in Fractures Filled with Viscous Fluid," Geophys., **73**(1), pp. N1–N7.
[5] Julian, B., 1994, "Volcanic Tremor: Nonlinear Excitation by Fluid Flow," J. Geophys. Res., **99**(B6), pp 11,859–11, 877.
[6] Balmforth, N. J., Craster, R. V., and Rust, A. C., 2005, "Instability in Flow Through Elastic Conduits and Volcanic Tremor," J. Fluid Mech., **527**, pp. 353–377.
[7] Tsai, V. C., and Rice, J. R., 2010, "A Model for Turbulent Hydraulic Fracture and Application to Crack Propagation at Glacier Beds," J. Geophys. Res., **115**.
[8] Geubelle, P. H., and Rice, J. R., 1995, "A Spectral Method for Three-Dimensional Elastodynamic Fracture Problems," J. Mech. Phys. Solids, **43**, pp. 1791–1824.
[9] Pedley, T. J., 1980, *The Fluid Mechanics of Large Blood Vessels*, Cambridge University Press, Cambridge.
[10] Rahman, M., and Barber, J. R., 1995, "Exact Expressions for the Roots of the Secular Equation for Rayleigh Waves," ASME J. Appl. Mech., **62**(1), pp. 250–252.
[11] Winberry, J. P., Anandakrishnan, S., and Alley, R. B., 2009, "Seismic Observations of Transient Subglacial Water-Flow Beneath MacAyeal Ice Stream, West Antarctica," Geophys. Res. Lett., **36**.